

**KERNFORSCHUNGSZENTRUM  
KARLSRUHE**

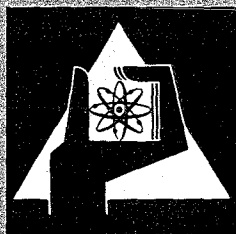
November 1972

KFK 1517  
EANDC(E) 146 „AL”

Institut für Angewandte Kernphysik  
Projekt Schneller Brüter

The Total Neutron Cross Sections of  $^{50}\text{Cr}$ ,  $^{52}\text{Cr}$ ,  $^{62}\text{Ni}$  and  $^{64}\text{Ni}$  in  
the Energy Region 10 – 300 keV

R.R. Spencer, H. Beer, F.H. Fröhner



GESELLSCHAFT  
FÜR  
KERNFORSCHUNG M.B.H.

KARLSRUHE

**Als Manuskript vervielfältigt**

**Für diesen Bericht behalten wir uns alle Rechte vor**

**GESELLSCHAFT FÜR KERNFORSCHUNG M. B. H.  
KARLSRUHE**

KERNFORSCHUNGSZENTRUM KARLSRUHE

KFK 1517

EANDC(E) 146 "AL"

Institut für Angewandte Kernphysik  
Projekt Schneller Brüter

The Total Neutron Cross Sections of  
 $^{50}\text{Cr}$ ,  $^{52}\text{Cr}$ ,  $^{62}\text{Ni}$  and  $^{64}\text{Ni}$  in the  
Energy Region 10 - 300 keV

R.R. Spencer, H. Beer, F.H. Fröhner

Gesellschaft für Kernforschung mbH, Karlsruhe



## ABSTRACT

Neutron total cross sections of  $^{50}\text{Cr}$ ,  $^{52}\text{Cr}$ ,  $^{62}\text{Ni}$  and  $^{64}\text{Ni}$  have been determined in the energy region from 10 - 300 keV by means of transmission measurements on enriched samples. R-matrix fits to the transmission data were carried out and the parameters thus determined are presented.

Der totale Neutronenwirkungsquerschnitt von  $^{50}\text{Cr}$ ,  $^{52}\text{Cr}$ ,  $^{62}\text{Ni}$  und  $^{64}\text{Ni}$   
im Energiebereich von 10 - 300 keV

## ZUSAMMENFASSUNG

Die totalen Wirkungsquerschnitte von  $^{50}\text{Cr}$ ,  $^{52}\text{Cr}$ ,  $^{62}\text{Ni}$  und  $^{64}\text{Ni}$  wurden im Energiebereich von 10 - 300 keV durch Transmissionsmessungen angereicherter Proben bestimmt. R-Matrix fits an die Transmissionsdaten wurden durchgeführt und die so bestimmten Parameter werden vorgelegt.

The Total Neutron Cross Sections of  $^{50}\text{Cr}$ ,  $^{52}\text{Cr}$ ,  $^{62}\text{Ni}$  and  $^{64}\text{Ni}$   
in the Energy Region 10 - 300 keV

INTRODUCTION

Transmission measurements on enriched samples of  $^{50}\text{Cr}$ ,  $^{52}\text{Cr}$ ,  $^{62}\text{Ni}$  and  $^{64}\text{Ni}$  have been carried out as part of a program to obtain a consistent set of resonance parameters which describe the neutron total and capture cross sections of reactor construction materials in the energy region of importance to the fast breeder development program. Previous measurements on these isotopes have been made with monochromatic neutron beams and did not include measurements of neutron capture  $\overline{1}$ ,  $\overline{2}$ ,  $\overline{3}$  or were made by time of flight techniques with linac produced neutrons  $\overline{4}$  which must contend with a severe  $\gamma$ -flash problem. Some disagreement in the derived resonance parameters from these previous experiments have resulted. It is felt that the present transmission measurements, along with measurements of neutron capture which are currently being analyzed, both made by time of flight techniques using the Kernforschungszentrum, Karlsruhe 3 MeV pulsed Van-de-Graaff will avoid many previous difficulties and result in a more acceptable set of resonance parameters for reactor shielding and reactor design calculations.

EXPERIMENTAL METHOD

The transmission measurements were carried out by the time of flight technique over a flight path of 4.96 meters. Neutrons were produced by means of the  $\text{Li}^7(p,n)\text{Be}^7$  reaction in a thick lithium target with the 1 nsec wide proton bursts from a pulsed Van-de-Graaff-accelerator operated at a repetition rate of 250 kHz. The neutrons were detected by a  $4\frac{3}{8}$ " dia x  $1/2$ " thick  $^6\text{Li}$  loaded glass scintillator<sup>+) and XP 1040 photomultiplier. A more detailed description of this detector appears elsewhere  $\overline{5}$ .</sup>

---

<sup>+) Nuclear Enterprises NE 905</sup>

Flight times of the neutrons were determined and recorded with a Laben digital time sorter and a CAE 510 on-line computer. Samples and an identical empty sample holder were cycled into the beam approximately every 15 minutes to average out beam fluctuations, the cycling period being determined by the proton beam integrator. The samples consisted of enriched metals or oxides placed in 1.1 cm diameter thin-walled aluminium containers. The sample thicknesses used and the isotopic composition of all samples are given in Table I. During analysis of the data it was found difficult to fit the shape of the low-energy transmission maximum of s-wave resonances in the measurements on the oxide samples. Chemical analysis of the  $^{52}\text{Cr}$ -oxide showed a 0.38 %  $\text{H}_2\text{O}$  contaminant. This weight percent  $\text{H}_2\text{O}$  was assumed for all the  $^{52}\text{Cr}$  and  $^{50}\text{Cr}$  samples, resulting in improved theoretical fits to the data in all cases.

TABLE I:

Sample Material <sup>+</sup>		Isotopic Composition (Atomic Fraction)	
Thick:	6.90 g $\text{Cr}_2\text{O}_3$	0.9680	$^{50}\text{Cr}$
		0.0298	$^{52}\text{Cr}$
Thin:	4.02 g $\text{Cr}_2\text{O}_3$	0.0018	$^{53}\text{Cr}$
		0.0004	$^{54}\text{Cr}$
Thick:	13.05 g $\text{Cr}_2\text{O}_3$	0.9974	$^{52}\text{Cr}$
		0.0002	$^{50}\text{Cr}$
Thin:	7.96 g $\text{Cr}_2\text{O}_3$	0.0023	$^{53}\text{Cr}$
		0.0001	$^{54}\text{Cr}$
Thick:	8.49 g Ni	0.9875	$^{62}\text{Ni}$
		0.0047	$^{58}\text{Ni}$
Thin:	5.07 g Ni	0.0056	$^{60}\text{Ni}$
		0.0022	$^{61}\text{Ni}$
Thick:	10.63 g Ni	0.9792	$^{64}\text{Ni}$
		0.0092	$^{58}\text{Ni}$
Thin:	4.24 g Ni	0.0073	$^{60}\text{Ni}$
		0.0005	$^{61}\text{Ni}$
		0.0038	$^{62}\text{Ni}$

<sup>+</sup> Samples were obtained through the USAEC-EANDC loan pool.

RESULTS

Transmissions and their statistical uncertainties were computed from the data by means of the FORTRAN IV code TRAMI [6]. The sample and open backgrounds for these calculations are determined from the counts in the sample and open spectra, respectively, in a region between the  $\gamma$ -ray peak and the onset of the fastest neutrons. Measurements on several "black" resonances in the energy region below 50 keV showed no indication of a time dependent background, thus the above method of background determination is felt to be reasonable. Chi-square fits to the transmission data were then calculated using an R-matrix formalism such as that reviewed by Lane and Thomas [7]. These fits and the final plotting routines were carried out by means of the code Fanal II [8]. This program accepts an initial set of parameters for the major isotopes of the sample, including contaminants, computes resolution broadened cross sections and then transmissions at neutron energies corresponding to the measured data. The chi-square error is calculated and preselected parameters are "wiggled". The calculations are then repeated until the relative change in  $\chi^2$  is less than a prescribed amount, i.e.,

$$\frac{\chi_i^2 - \chi_{i-1}^2}{\chi_{i-1}^2} < \epsilon$$

where

$$\chi_i^2 = \sum_{n=1}^N \left[ \frac{T_n - \bar{T}(i, E_n)}{\delta T_n} \right]^2$$

and  $T_n$  = measured transmission at energy  $E_n$ ,  $\delta T_n$  is its uncertainty, and  $\bar{T}(i, E_n)$  is the computed transmission. The resolution function is assumed to be a Gaussian

$$R(E, E') dE' = \frac{1}{W \sqrt{\pi}} e^{-(t-t')^2/W^2} dt'$$

where for the present measurements,

$$W^2 = 4.42 + 1.14 \times 10^{-6} t^2$$

and  $t$  is the flight time in nsec. Doppler broadening was assumed to be negligible. Neutron energies were computed from their time of flight using the  $\gamma$ -ray peak position to determine time zero.

In the case of the oxide samples, the oxygen cross-section was included by means of a potential scattering radius of 5.6 fermis as a contaminant input. This produced a slightly energy dependent cross-section for oxygen below 300 keV which is in good agreement with the data of Mooring et al. [9]. The hydrogen contribution from the water contaminant was taken into account by means of the formula of Gammel [10].

The resulting best fits to the transmission data are shown with the measured thick and thin sample data points in the lower diagrams of figures 1 through 8. For the sake of clarity error bars indicating the statistical uncertainty in the measured data were plotted for every 10<sup>th</sup> or 20<sup>th</sup> point, only. The upper diagrams of figures 1 through 8 are plots of the resolution-broadened, total cross sections for the pure isotopes,  $^{50}\text{Cr}$ ,  $^{52}\text{Cr}$ ,  $^{62}\text{Ni}$  and  $^{64}\text{Ni}$ . These cross sections were computed from the derived R-matrix parameters given in tables II through V.<sup>+)</sup> In these tables are listed the values and estimated errors for the resonance energies,  $E_0$ , and the neutron widths,  $\Gamma_n$ , (or  $g\Gamma_n$  for  $l > 0$ ). Also given are values of  $a_J$ , the s-wave potential scattering parameter, and  $S_J$ , a parameter which describes the effect of distant resonances.  $S_J$  is the strength function of a "Picket Fence" model which assumes equally spaced resonances of equal widths outside the region of analysis. Since two separate energy regions were required in these experiments, two values of the parameters  $A_J$  and  $S_J$  were obtained for each isotope and are given in the tables with their respective energy regions.

---

<sup>+)</sup> Sets of total cross section values calculated from the resonance parameters and valid for the pure isotopes can be requested from the neutron data center at Saclay (Postal address: CCDN, B.P. 9, F-91 Gif-sur-Yvette, France).

TABLE II -  $^{50}\text{Cr}$  Target

$E_o$ (keV)	$g \Gamma_n$ (keV)	$l$
28.43 $\pm$ .09	0.415 $\pm$ .010	0
37.32 $\pm$ .12	2.24 $\pm$ .03	0
54.99 $\pm$ .18	0.281 $\pm$ .017	0
64.8 $\pm$ .2	0.043 $\pm$ .020	0
94.75 $\pm$ .4	1.67 $\pm$ .05	0
111.8 $\pm$ .5	0.09 $\pm$ .05	> 0
114.8 $\pm$ .5	0.12 $\pm$ .05	0
129.0 $\pm$ .6	0.54 $\pm$ .08	0
156.6 $\pm$ .7	1.23 $\pm$ .11	0
162.45 $\pm$ .8	0.75 $\pm$ .10	0
185.2 $\pm$ .9	3.52 $\pm$ .14	0
218.3 $\pm$ 1.2	0.17 $\pm$ .13	0
231.6 $\pm$ 1.2	0.94 $\pm$ .15	0
245.6 $\pm$ 1.4	0.20 $\pm$ .15	0
276.6 $\pm$ 1.5	1.9 $\pm$ .2	0
289.8	3.7	0

$E_n < 117$  keV

$a_J = 4.7$  fm

$S_J = 0$

$E_n > 117$  keV

$a_J = 4.2$  fm

$S_J = 5 \times 10^{-4}$

TABLE III -  $^{52}\text{Cr}$  Target

$E_o$ (keV)	$g \Gamma_n$ (keV)	$l$
22.92 ± .07	≈ 0.005	> 0
31.62 ± .10	0.015 ± .008	0
50.19 ± .16	1.71 ± .02	0
57.6 ± .2	0.079 ± .017	> 0
96.2 ± .4	6.40 ± .06	0
106.0 ± .4	0.06 ± .04	> 0
111.6 ± .5	0.06 ± .05	> 0
118.1 ± .5	≈ 0.03	0
121.4 ± .5	0.61 ± .06	0
130.1 ± .6	0.22 ± .06	> 0
139.7 ± .6	5.4 ± .2	0
141.3 ± .6	0.7 ± .2	0
234.0 ± 1.3	0.3 ± .2	> 0
235.8 ± 1.3	1.1 ± .2	> 0
242.6 ± 1.4	0.22 ± .15	> 0
246.3 ± 1.4	1.01 ± .16	> 0
249.3 ± 1.4	0.55 ± .16	0
256.7 ± 1.5	0.31 ± .17	> 0
281.9 ± 1.6	0.55 ± .19	> 0

$E_n < 90 \text{ keV}$

$a_J = 4.5 \text{ fm}$

$S_J = 1.5 \times 10^{-4}$

$E_n > 90 \text{ keV}$

$a_J = 4.4 \text{ fm}$

$S_J = 3 \times 10^{-4}$

TABLE IV -  $^{62}\text{Ni}$  Target

$E_o$ (keV)	$g \Gamma_n$ (keV)	$l$
$42.87 \pm .14$	$0.340 \pm .015$	0
$56.91 \pm .19$	$0.056 \pm .017$	> 0
$77.2 \pm .3$	$0.07 \pm .03$	0
$78.4 \pm .3$	$0.05 \pm .03$	> 0
$94.7 \pm .4$	$2.5 \pm .1$	0
$105.6 \pm .4$	$4.6 \pm .2$	0
$149.3 \pm .7$	$0.14 \pm .07$	0
$188.2 \pm .9$	$\approx 0.09$	0
$214.7 \pm 1.1$	$0.19 \pm .13$	0
$229.5 \pm 1.2$	$6.18 \pm .16$	0
$243.2 \pm 1.3$	$0.78 \pm .15$	0
$281.1 \pm 1.6$	$4.8 \pm .4$	0
$\approx 288.0$	$\approx 1.00$	0

$E_n < 90$  keV

$a_J = 6.0$  fm

$S_J = 7.8 \times 10^{-4}$

$E_n > 90$  keV

$a_J = 6.5$  fm

$S_J = 4.1 \times 10^{-4}$

TABLE V -  $^{64}\text{Ni}$  Target

$E_o$ (keV)	$g \Gamma_n$ (keV)	$l$
14.3 ± .2	2.9 ± .5	0
33.82 ± .10	8.90 ± .05	0
106.5 ± .4	0.11 ± .05	> 0
129.3 ± .5	1.34 ± .07	0
142.0 ± .6	0.17 ± .07	> 0
148.8 ± .7	0.08 ± .07	0
155.0 ± .7	3.9 ± .1	0
163.2 ± .8	0.14 ± .08	0
177.7 ± .8	0.47 ± .09	0
191.5 ± .9	0.16 ± .11	> 0
205.3 ± 1.1	≈ 0.06	0
214.7 ± 1.1	≈ 0.08	> 0
219.8 ± 1.1	≈ 0.03	0
226.9 ± 1.2	≈ 0.12	0
231.9 ± 1.2	3.77 ± .16	0
237.9 ± 1.3	0.32 ± .13	> 0
255.7 ± 1.4	0.17 ± .15	> 0
269.7 ± 1.5	2.2 ± .2	0
283.5 ± 1.6	0.35 ± .19	0

$E_n < 98$  keV

$a_J = 6.4$  fm

$S_J = 3.4 \times 10^{-4}$

$E_n > 98$  keV

$a_J = 6.4$  fm

$S_J = 1.6 \times 10^{-4}$

DISCUSSION

A comparison of the  $^{50}\text{Cr}$  and  $^{52}\text{Cr}$  results with data of other authors indicates some significant differences in the energy measurement at different facilities. In particular the time of flight measurements of ref. [4] using electron linac produced neutrons show a systematic disagreement with the resonance energies of Tables II and III, (virtually no difference at the lowest energies, approximately 1 keV at 100 keV neutron energy and approximately 5 keV at 280 keV neutron energy), the energies of ref. [4] being consistently higher. Within the rather broad error limits this energy difference varies as  $E^{3/2}$  suggesting a constant error in one or the other time scale such as incorrect location of the zero of time would cause. In the present data the  $\gamma$ -ray peak is recorded in the neutron time of flight spectrum and is used directly to compute the zero of time. The  $^{53}\text{Cr}$  energy data of Müller and Rohr [11] taken with the KFK Van-de-Graaff and with a different flight path and detector from the present experiments show a similar relationship to the  $^{53}\text{Cr}$  resonance energies of ref. [4].

On the other hand, the  $^{50}\text{Cr}$ ,  $^{62}\text{Ni}$  and  $^{64}\text{Ni}$  data of ref. [3], taken with monoenergetic neutrons produced by a Van-de-Graaff, show a small, approximately constant (with energy) shift in resonance energies for each isotope of  $\leq 1$  keV compared to the present results on these same isotopes. The  $^{50}\text{Cr}$  resonance energies of ref. [3] are higher whereas their  $^{62}\text{Ni}$  and  $^{64}\text{Ni}$  resonance energies are lower than ours. This is relatively good agreement considering the ref. [3] energies are based on a neutron threshold measurement and contain an uncertainty due to the  $^7\text{Li}$  target thickness.

A recent report of Garg et.al. [12] gives  $^{62}\text{Ni}$  resonance parameters which these authors have derived from transmission measurements on natural nickel samples. Our results on separated  $^{62}\text{Ni}$  samples clearly show that there is no resonance in  $^{62}\text{Ni}$  with a width as large as .25 keV near 89 keV neutron energy as reported in [12]. On the other hand the present data show several additional  $^{62}\text{Ni}$  resonances which were not observed in the natural nickel transmission data [12]. The neutron widths reported here are in fair agreement with those of previous authors [1,2,3,4].

Although there are some discrepancies outside quoted errors in some individual neutron widths, the s-wave strength function values for  $^{50}\text{Cr}$

and  $^{52}\text{Cr}$  computed from the present data are in very good agreement with those reported in ref.  $\overline{[4]}$ . The present values are listed in Table VI along with the s-wave strength functions derived from the  $^{62}\text{Ni}$  and  $^{64}\text{Ni}$  data. Some values of other authors are included for comparison.

TABLE VI - s-wave strength functions

Target Nucleus	Experimental Strength Function ( $S_0 \times 10^{-4}$ )	
$^{50}\text{Cr}$	$1.7 \pm 0.7$	$2.18 \pm 0.75^{4)}$
$^{52}\text{Cr}$	$1.9 \pm 1.0$	$2.10 \pm 1.05^{4)}$
$^{62}\text{Ni}$	$1.8 \pm 0.9$	$2.9 \pm 0.8^{13)}$ compilation
$^{64}\text{Ni}$	$3.5 \pm 1.4$	$2.0 \pm 0.7^{13)}$ compilation

For  $^{50}\text{Cr}$  the present  $g \Gamma_n$  values appear to be in better agreement with the results of ref.  $\overline{[4]}$  than those of ref.  $\overline{[3]}$ . Our somewhat lower value for the width of the  $^{50}\text{Cr}$  (94.7 keV) resonance may be due to our direct inclusion in the analysis of the broad  $^{52}\text{Cr}$  resonance nearby as a contaminant. For  $^{52}\text{Cr}$  the present results and those of ref's.  $\overline{[3]}$  and  $\overline{[4]}$  are in fair agreement. It should be noted that the resonance near 140 keV in  $^{52}\text{Cr}$  was analyzed as a doublet in the present data. A singlet with  $\Gamma_n = 6.2$  keV also fits and may be preferred. For the isotopes  $^{62}\text{Ni}$  and  $^{64}\text{Ni}$  the present  $\Gamma_n$  values for s-wave resonances are in fair agreement with those of ref.  $\overline{[3]}$  although in general our values are lower.

Some remarks should be made with regard to spin assignments of particular resonances. The  $^{52}\text{Cr}$  (31.62 keV) resonance is reported here as s-wave although within the statistics of the data a higher  $\ell$ -wave shape would also fit. The  $^{62}\text{Ni}$  (56.91 keV) resonance is clearly not s-wave as suggested in ref.  $\overline{[3]}$ .

ACKNOWLEDGEMENTS:

The authors would like to express their appreciation for the high purity separated isotopes which were made available through the USAEC-EANDC loan pool and to the members of the KFK Van-de-Graaff operating staff who helped make this work possible.

REFERENCES

- [ 1 ] Newson, H.W., Bilpuch, E.G., Karriker, F.P., Weston, L.W.,  
Patterson, J.R., and Bowman, C.D., Annals of Physics 14, 365 (1961).
- [ 2 ] Bowman, C.D., Bilpuch, E.G., and Newson, H.W., Annals of Physics  
17, 319 (1962).
- [ 3 ] Farrell, J.A., Bilpuch, E.G., and Newson, H.W., Annals of Physics  
37, 367 (1966).
- [ 4 ] Stieglitz, R.G., Hockenbury, R.W., and Block, R.C., Nuclear Physics  
A 163, 592 (1971).
- [ 5 ] Beer, H., Arbeitsbericht Nr. 99, KFK (unpublished).
- [ 6 ] Schneider, E., Arbeitsbericht Nr. 95/71, KFK (unpublished).
- [ 7 ] Lane, A.M., and Thomas, R.G., Rev. Mod. Phys. 30, 257 (1958).
- [ 8 ] Fröhner, F.H., Arbeitsbericht Nr. 97, KFK (unpublished).
- [ 9 ] Mooring, F.P., Monahan, J.E., and Huddleston, C.M., Nuclear Physics  
82, 16 (1966).
- [ 10 ] Gammel, J.L., Fast Neutron Physics, Part II, Chap. VI, p. 2185,  
Interscience Pub., Inc., New York (1960).
- [ 11 ] Müller, K.N., and Rohr, G., Nuclear Physics A 164, 97 (1971).
- [ 12 ] Garg, J.B., Rainwater, J., and Havens, W.W., Phys. Rev. C 3,  
2447, (1971).
- [ 13 ] Seth, K.K., Nucl. Data Sect. A 2, 299 (1966).

FIGURE CAPTIONS

- Fig. 1: (Below) - The transmission data and R-matrix fit for 0.073 and 0.126 nuclei/barn chromium-oxide samples, enriched in  $^{50}\text{Cr}$ , vs. neutron energy in the region 20 - 120 keV.  
(Above) - Resolution broadened, total cross-section for the pure isotope  $^{50}\text{Cr}$  computed from the R-matrix parameters.
- Fig. 2: (Below) - The transmission data and R-matrix fit for the  $^{50}\text{Cr}$  samples, vs. neutron energy in the region 120 - 290 keV.  
(Above) - Resolution broadened, total cross-section for the pure isotope  $^{50}\text{Cr}$  computed from the R-matrix parameters.
- Fig. 3: (Below) - The transmission data and R-matrix fit for 0.142 and 0.232 nuclei/barn chromium-oxide samples, enriched in  $^{52}\text{Cr}$ , vs. neutron energy in the region 27 - 90 keV.  
(Above) - Resolution broadened, total cross-section for the pure isotope  $^{52}\text{Cr}$  computed from the R-matrix parameters.
- Fig. 4: (Below) - The transmission data and R-matrix fit for the  $^{52}\text{Cr}$  samples, vs. neutron energy in the region 90 - 290 keV.  
(Above) - Resolution broadened, total cross-section for the pure isotope  $^{52}\text{Cr}$  computed from the R-matrix parameters.
- Fig. 5: (Below) - The transmission data and R-matrix fit for 0.044 and 0.073 nuclei/barn nickel samples, enriched in  $^{62}\text{Ni}$ , vs. neutron energy in the region 27 - 90 keV.  
(Above) - Resolution broadened, total cross-section for the pure isotope  $^{62}\text{Ni}$  computed from the R-matrix parameters.
- Fig. 6: (Below) - The transmission data and R-matrix fit for the  $^{62}\text{Ni}$  samples, vs. energy in the region 90 - 290 keV.  
(Above) - Resolution broadened, total cross-section for the pure isotope  $^{62}\text{Ni}$  computed from the R-matrix parameters.

Fig. 7: (Below) - The transmission data and R-matrix fit for the 0.035 nuclei/barn nickel sample, enriched in  $^{64}\text{Ni}$ , vs. neutron energy in the region 16 - 98 keV.

(Above) - Resolution broadened, total cross-section for the pure isotope  $^{64}\text{Ni}$  computed from the R-matrix parameters.

Fig. 8: (Below) - The transmission data and R-matrix fit for the 0.035 and 0.089 nuclei/barn  $^{64}\text{Ni}$  enriched samples, vs. neutron energy in the region 98 - 290 keV.

(Above) - Resolution broadened, total cross-section for the pure isotope  $^{64}\text{Ni}$  computed from the R-matrix parameters.



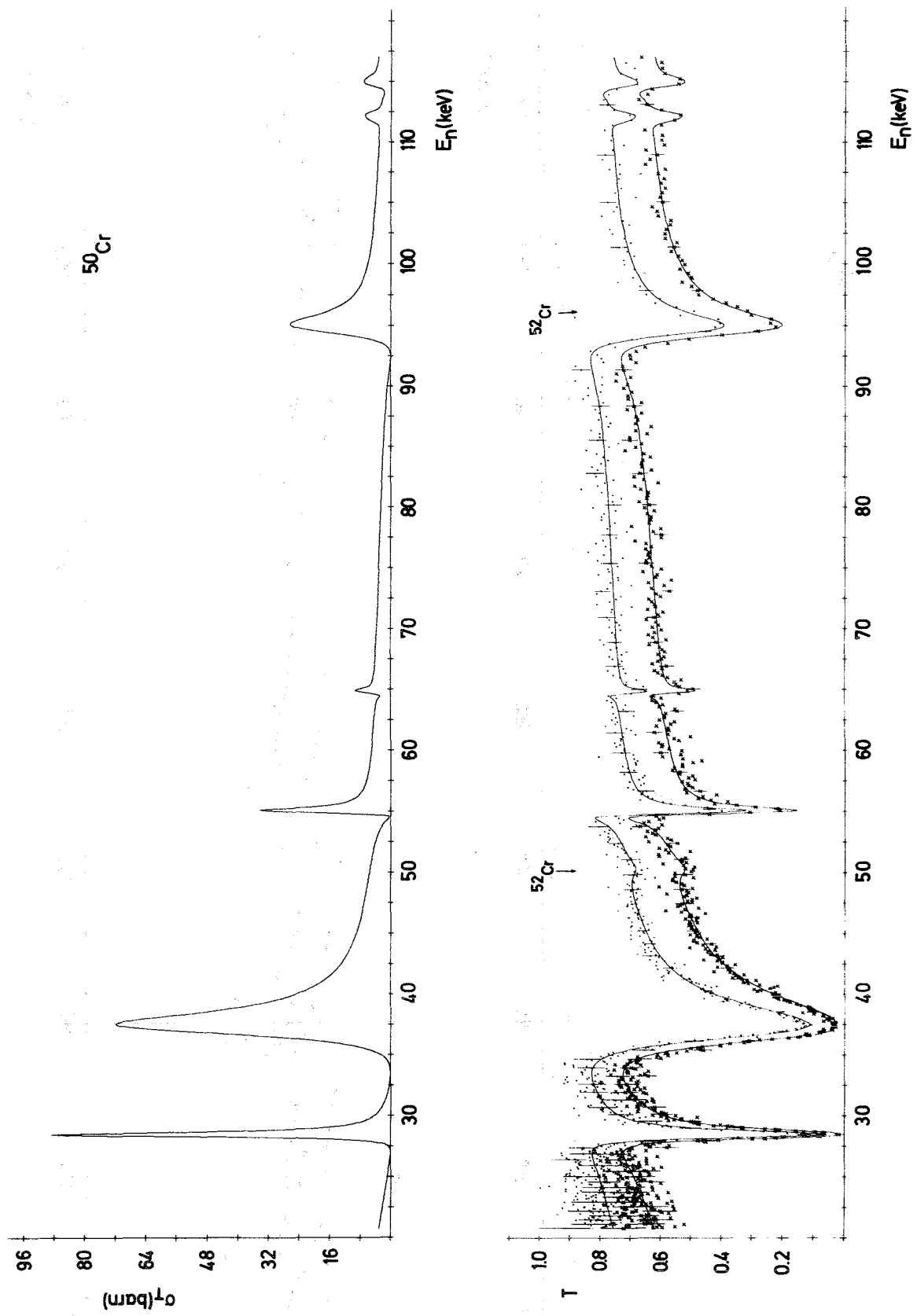


Fig. 1

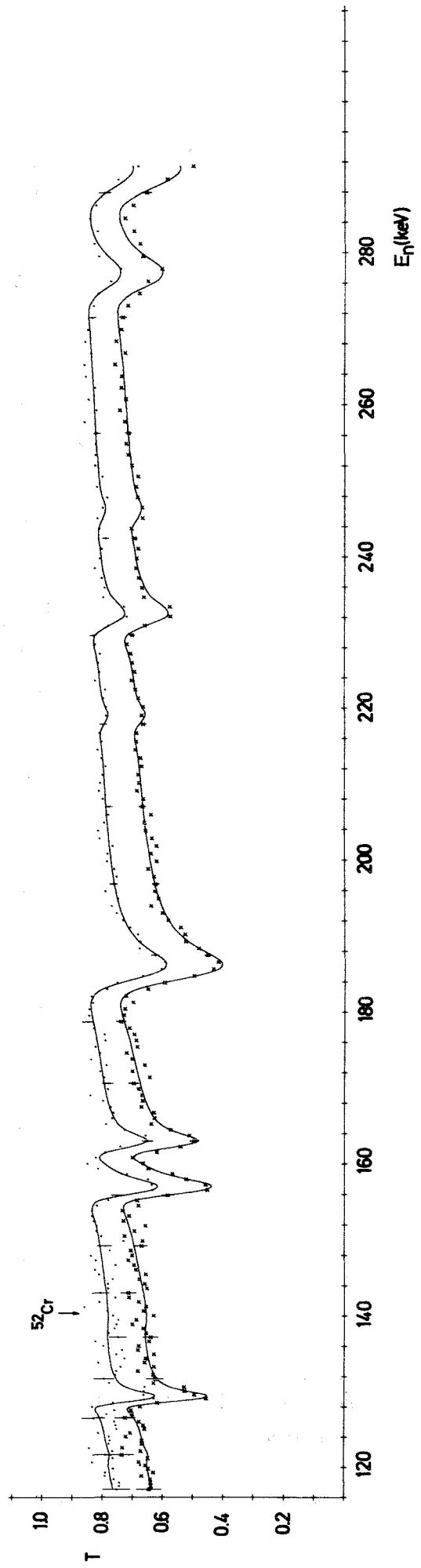
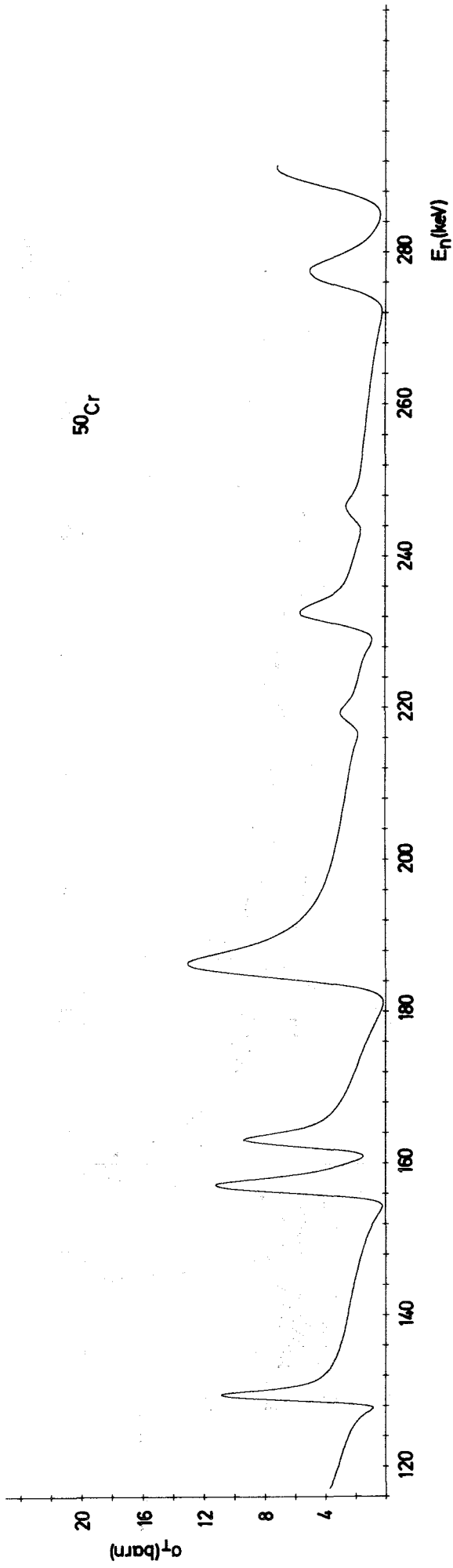


Fig. 2

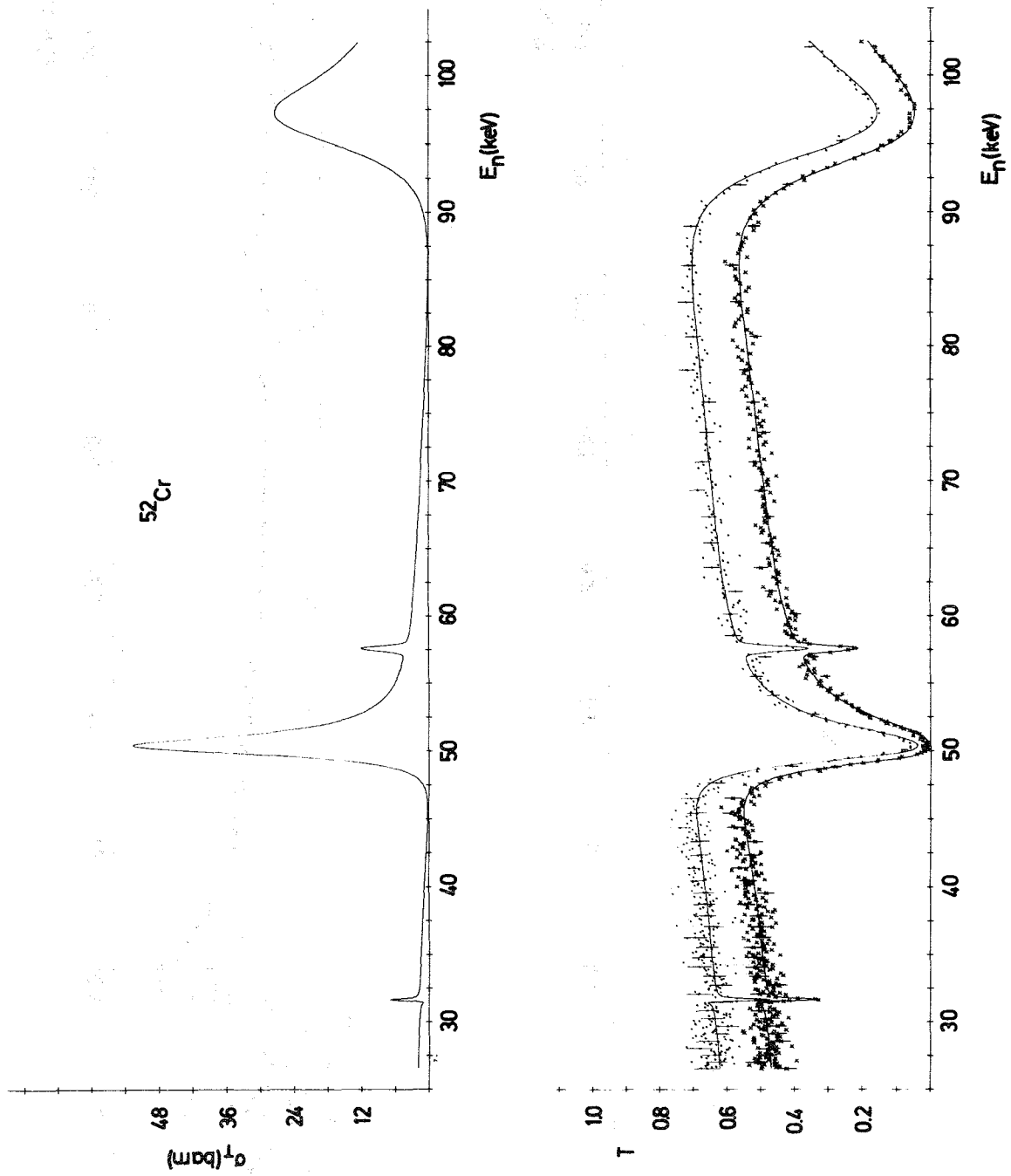


Fig. 3

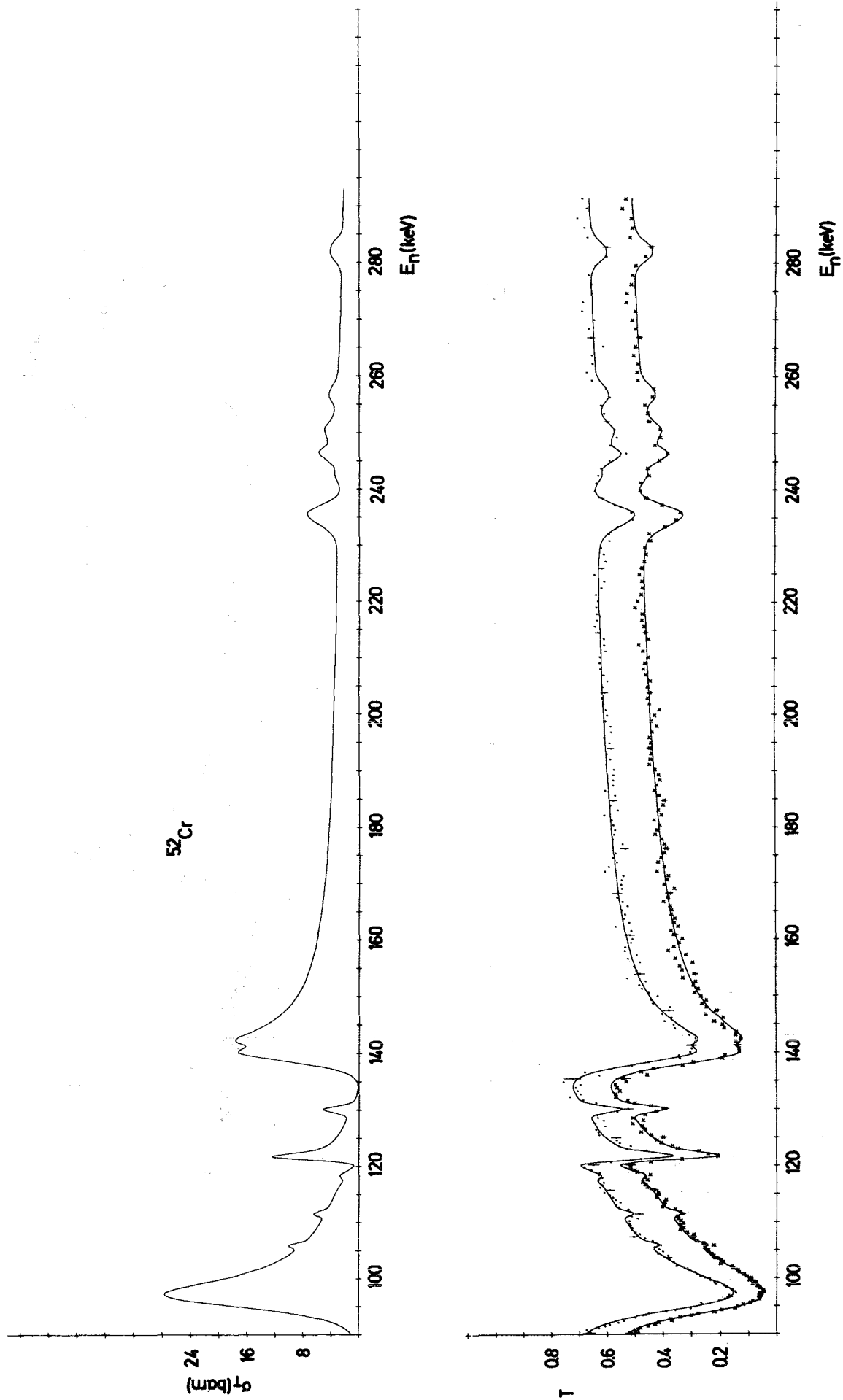


Fig. 4

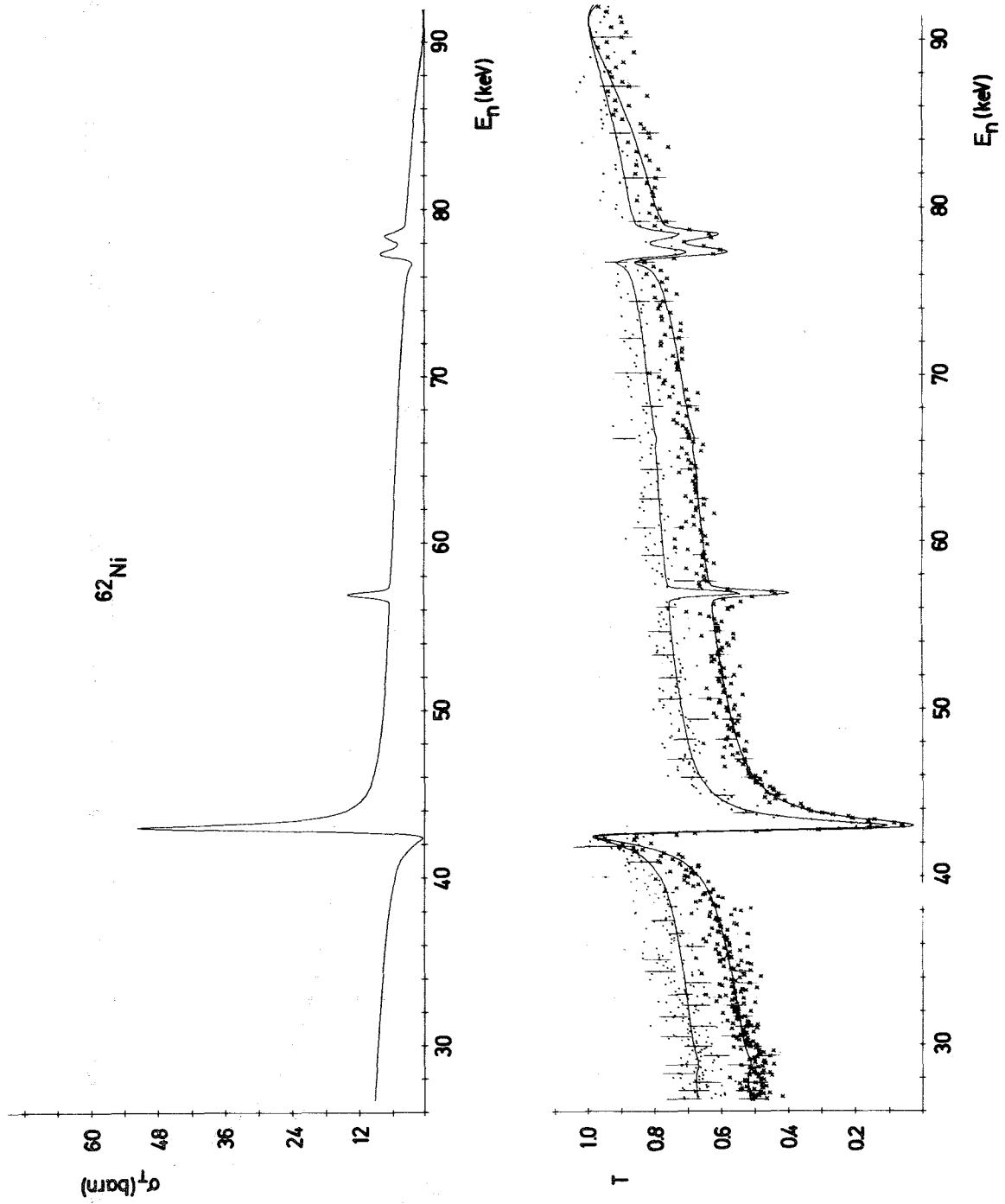


Fig. 5

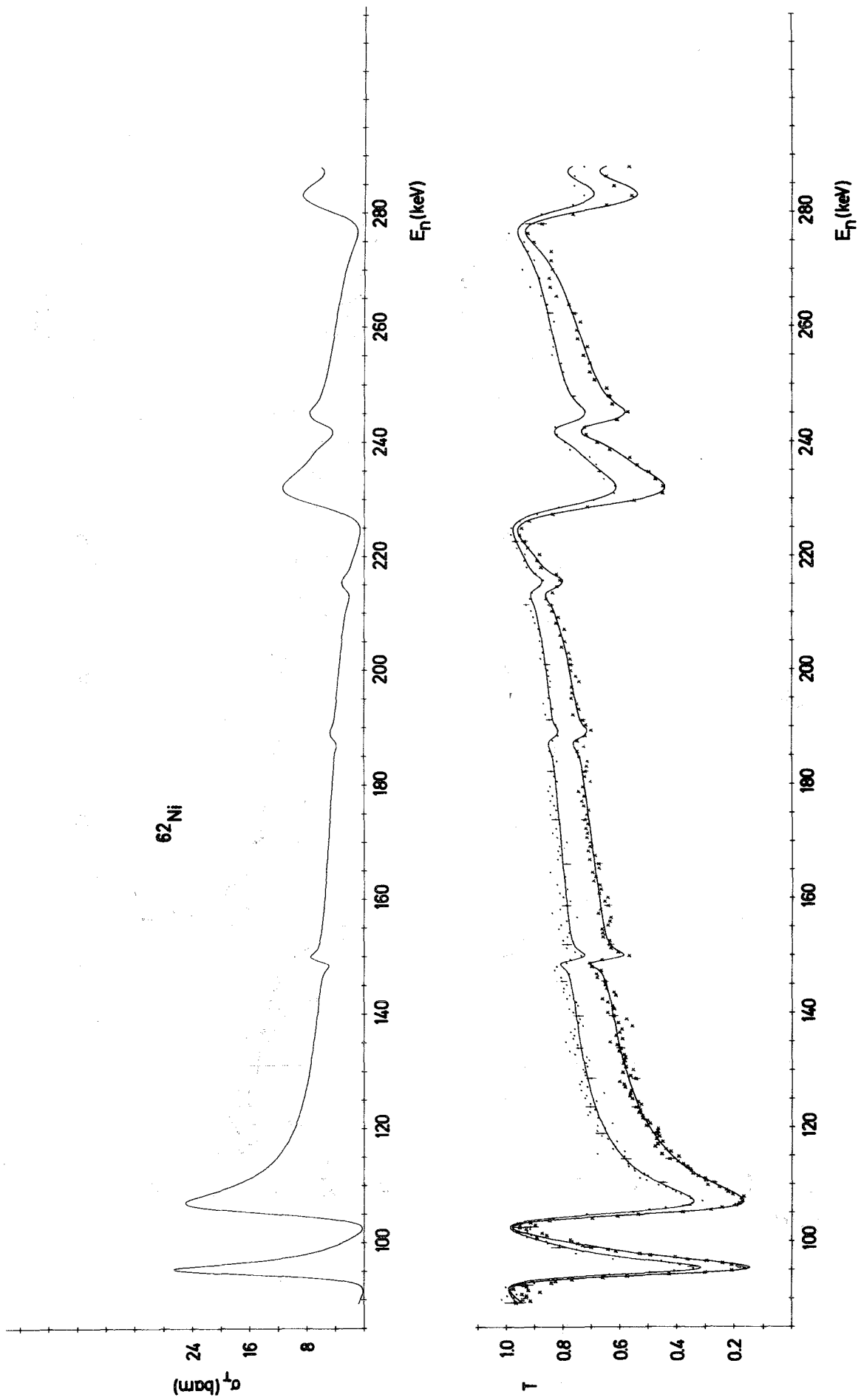


Fig. 6

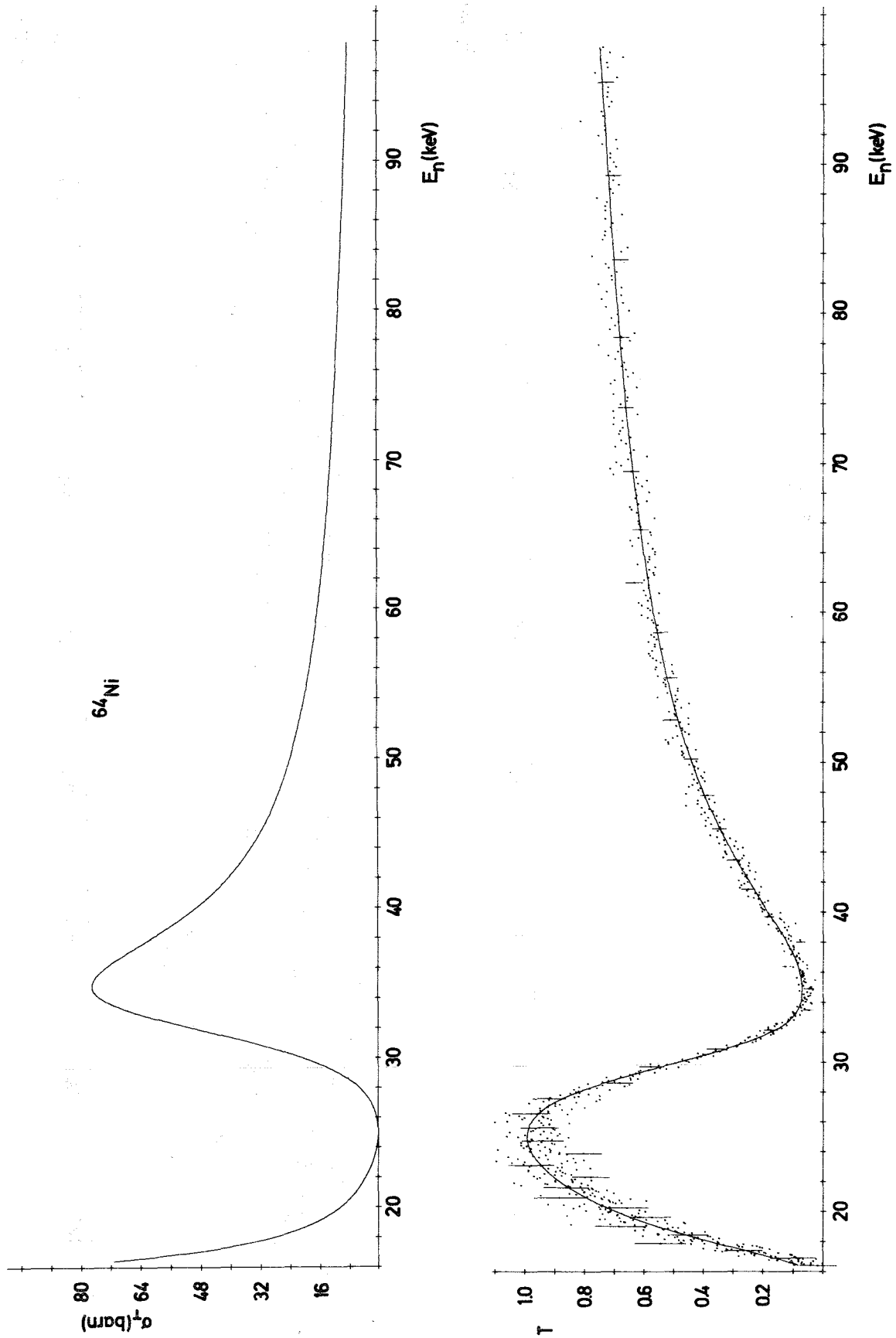


Fig. 7

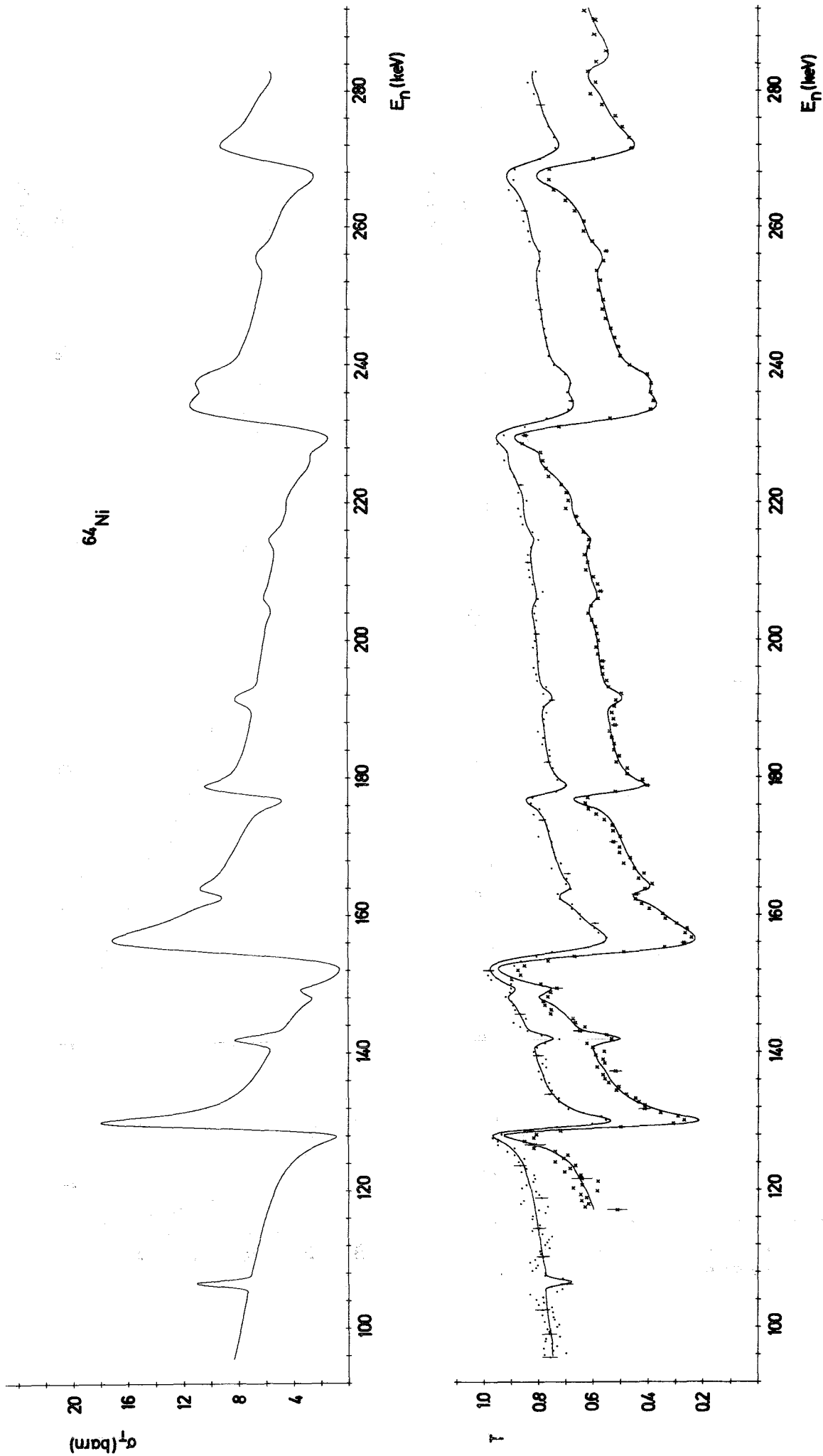


Fig. 8